

1 **Assessment of Neurovascular Coupling & Cortical Spreading Depression in Mixed Models of  
2 Atherosclerosis & Alzheimer's Disease**

3 Osman Shabir<sup>1,2,3</sup>, Ben Pendry<sup>4</sup>, Llywelyn Lee<sup>2,3</sup>, Beth Eyre<sup>2,3</sup>, Paul Sharp<sup>2</sup>, Monica A Rebollar<sup>3,4</sup>, Clare  
4 Howarth<sup>2,3</sup>, Paul R Heath<sup>3,4</sup>, Stephen B Wharton<sup>3,4</sup>, Sheila E Francis<sup>1,3,5†</sup> & Jason Berwick<sup>2,3,5†\*</sup>

5

6 *†Authors Contributed Equally.*

7 \*Corresponding Author: Dr Jason Berwick, Sheffield Neurovascular Lab, Department of Psychology,  
8 The University of Sheffield, Alfred Denny Building, Western Bank, Sheffield, S10 2TN (United Kingdom).  
9 Email: [j.berwick@sheffield.ac.uk](mailto:j.berwick@sheffield.ac.uk) Phone: (+44) 0114 222 6597

10

11 Author Affiliations:

12 <sup>1</sup>Department of Infection, Immunity & Cardiovascular Disease (IICD), University of Sheffield Medical  
13 School, Royal Hallamshire Hospital, Beech Hill Road, Sheffield, S10 2RX (United Kingdom)

14 <sup>2</sup>Sheffield Neurovascular Lab, Department of Psychology, University of Sheffield, Alfred Denny  
15 Building, Western Bank, Sheffield, S10 2TN (United Kingdom)

16 <sup>3</sup>Neuroscience Institute, University of Sheffield, Sheffield, S10 2TN (United Kingdom)

17 <sup>4</sup>Sheffield Institute for Translational Neuroscience (SITraN), University of Sheffield, 385a Glossop  
18 Road, Sheffield, S10 2HQ (United Kingdom)

19 <sup>5</sup>Healthy Lifespan Institute (HELSI), University of Sheffield, Sheffield, S10 2TN (United Kingdom)

20

21 **Key Words:** Neurovascular coupling, atherosclerosis, Alzheimer's disease, CSD, comorbid

22

23 **Abstract**

24 Neurovascular coupling is a critical brain mechanism whereby changes to blood flow accompany  
25 localised neural activity. The breakdown of neurovascular coupling is linked to the development and  
26 progression of several neurological conditions including dementia. In this study, we examined cortical  
27 haemodynamics in preparations that modelled Alzheimer's disease (J20-AD) and atherosclerosis  
28 (PCSK9-ATH) between 9-12m of age. We report novel findings with atherosclerosis where  
29 neurovascular decline is characterised by significantly reduced blood volume, levels of oxyhaemoglobin  
30 & deoxyhaemoglobin, in addition to global neuroinflammation. In the comorbid mixed model (J20-  
31 PCSK9-MIX), we report a 3x fold increase in hippocampal amyloid-beta plaques. A key finding was that  
32 cortical spreading depression (CSD) due to electrode insertion into the brain was worse in the diseased  
33 animals and led to a prolonged period of hypoxia. These findings suggest that systemic atherosclerosis  
34 can be detrimental to neurovascular health and that having cardiovascular comorbidities can  
35 exacerbate pre-existing Alzheimer's-related amyloid-plaques.

36

37 **Introduction**

38 Alzheimer's disease (AD) is the most common form of dementia worldwide, with the vast majority of  
39 cases being sporadic and occurring 65 years and over. Population based studies have shown that AD  
40 and vascular pathologies commonly coexist in the brains of elderly individuals (Kapasi et al., 2017;

1 Matthews et al., 2009; Neuropathology Group. Medical Research Council Cognitive & Aging, 2001;  
2 Rahimi & Kovacs, 2014). A major cardiovascular pathology that affects as many as up to 60% of all  
3 individuals after the age of 55 is atherosclerosis. Atherosclerosis is the progressive thickening,  
4 hardening and narrowing of major arteries, including those that supply the brain, such as the carotids  
5 (Lusis, 2000). Intracranial atherosclerosis does not occur until much later in life, around 75 years and  
6 above. As such, Alzheimer's disease that begins around the 8<sup>th</sup> decade of life is usually present with  
7 other comorbidities such as atherosclerosis (Napoli et al., 1999). There is also evidence that, not only  
8 do these often exist as comorbidities, but they may interact pathogenically with vascular disease and  
9 neurovascular unit changes contributing to AD (Iadecola, 2017; Kapasi & Schneider, 2016). To date,  
10 there are very limited models of comorbidity with respect to preclinical studies, and instead models have  
11 been very specific and 'pure', and not reflective of the clinical pathology in humans. Atherosclerosis is  
12 known to be a major risk factor for the development of dementia. The progressive atheromatous plaque  
13 build-up within cerebral arteries that supply the cortex over time can lead to stenosis producing  
14 insufficient oxygen delivery to the brain parenchyma, potentially resulting in neuronal death and  
15 symptoms of dementia (Shabir et al., 2018). Indeed, the vascular cognitive impairment (VCI) which  
16 precedes the onset of dementia may be attributed to a variety of different vascular pathologies affecting  
17 either systemic or intracranial vasculature (both large or small vessels) (Iadecola et al., 2019). Due to  
18 the complexity of atherosclerosis and dementia pathogenesis, understanding the mechanisms of their  
19 mutual interactions is necessary if efforts to develop therapeutics to prevent VCI and vascular dementia,  
20 which currently has no disease-modifying cure, are to succeed.

21  
22 The breakdown of NVC is thought to be an important and early pathogenic mechanism in the onset and  
23 progression of a range of neurological conditions (Zlokovic, 2011). In the present study, we aimed to  
24 investigate neurovascular function in mid-aged (9-12m old) mice where atherosclerosis was a  
25 comorbidity. We used a novel model of atherosclerosis that utilises a single adeno-associated virus  
26 (AAV) i.v. injection of a gain of function mutation (D377Y) to proprotein convertase subtilisin/kexin type  
27 9 (rAAV8-mPCSK9-D377Y), combined with a high-fat Western diet to induce atherosclerosis in most  
28 adult mouse strains (Bjorklund et al., 2014; Roche-Molina et al., 2015). This leads to the constitutively  
29 active inhibition of the LDL-receptor preventing cholesterol internalisation and degradation by  
30 hepatocytes, leading to hypercholesterolaemia to occur and the development of robust atherosclerotic  
31 lesions within 6-8 weeks (Bjorklund et al., 2014). Furthermore, in order to address the effect  
32 atherosclerosis could have on mild Alzheimer's pathology, we combined the atherosclerosis with the  
33 mild J20-hAPP mouse model of familial Alzheimer's disease (fAD) to create a mixed comorbid mouse  
34 model (J20-PCSK9-MIX). The J20-hAPP mouse model of fAD over-expresses human amyloid  
35 precursor protein (hAPP) with the Swedish (K670N and M671L) and the Indiana (V717F) familial  
36 mutations (Mucke et al., 2000), which begin to develop amyloid-beta (A $\beta$ ) plaques around 5-6 months  
37 of age, and show signs of cognitive impairments from 4 months (Ameen-Ali et al., 2019). We  
38 hypothesised that atherosclerosis would exacerbate Alzheimer's disease pathology in the brain and  
39 that neurovascular function would be further worsened compared to AD or ATH models alone. We have  
40 previously reported no significant alterations to evoked-haemodynamics in the J20-AD model of the

1 same age (9-12m); however, under acute imaging sessions where an electrode was inserted into the  
2 brain, we found significantly perturbed haemodynamics (Sharp et al., 2019). We hypothesised that  
3 electrode insertion causes cortical spreading depression (CSD). Based on recent data linking migraine  
4 with aura with cardiovascular disease (Kurth et al., 2020), we hypothesised that experimental CSD  
5 might be heightened in all disease models. We report that experimentally induced atherosclerosis in  
6 the J20-AD model increased the number of A $\beta$  plaques by 300%. Furthermore, experimental CSD is  
7 more severe in all diseased groups compared to WT controls.

8

## 9 **Results**

### 10 2D-Optical Imaging Spectroscopy (2D-OIS) Measures Brain Cortical Haemodynamics Through a 11 Thinned Cranial Window

12 We performed chronic imaging of the brain cortex 3-weeks post-surgery, where the thinned cranial  
13 window remained intact (Figure 1A/B), as described previously (Shabir et al., 2020; Sharp et al., 2019).  
14 We deployed a range of stimulations (2s & 16s mechanical whisker stimulations) with the mouse  
15 breathing both 100% oxygen (hyperoxia) and 21% oxygen (normoxia), in addition to recording  
16 transitions between conditions and performing a 10% hypercapnia test to test the maximum dilation of  
17 vessels. Each experimental day consisted of the same set of experiments with consistent timings to  
18 ensure reliability across all animal groups. First, a 2s-whisker stimulation (5Hz) with the mouse  
19 breathing 100% oxygen; hyperoxia, consisting of 30 trials, second, a 16s-whisker stimulation consisting  
20 of 15 trials. Animals were then transitioned from hyperoxia to 21% oxygen; normoxia, and the baseline  
21 haemodynamic changes were recorded. The same set of stimulations were deployed under normoxia  
22 (2s & 16s stimulations), before transitioning back to hyperoxia for a final 10% hypercapnia test. Using  
23 these stimulations, activation maps of blood volume; total haemoglobin (HbT), can be generated (Figure  
24 1C). Mice were allowed to recover and after 1-week, a final acute imaging session was performed. In  
25 this setup, a small burr-hole was drilled through the thinned skull overlying the active region of interest  
26 (ROI) as determined from the chronic imaging sessions (Figure 1D), and a multichannel electrode was  
27 inserted into the brain (Figure 1E) to record neural activity simultaneously. We then imaged and  
28 recorded the baseline haemodynamics for a 35-minute period to observe the effect electrode insertion,  
29 before commencing the first stimulation. This was also done to record baselines on chronic imaging  
30 sessions.

31

### 32 Chronic Haemodynamic Responses in the Brain are Reduced in PCSK9-ATH Mice

33 Cortical haemodynamics were imaged through a thinned cranial window to determine whether evoked  
34 cortical haemodynamics were different between 9-12m old wild-type (WT), atherosclerotic (PCSK9-  
35 ATH), Alzheimer's (J20-AD) & mixed (J20-PCSK9-MIX) mouse models (Figure 2). Across all  
36 stimulations and conditions, ATH-PCSK9 mice displayed a significant reduction of evoked blood volume  
37 responses (HbT; peak value) compared to WT controls. J20-AD mice and J20-PCSK9-MIX mice did  
38 not exhibit a significant change in HbT across all stimulation conditions compared to WT mice. Evoked  
39 HbT responses; although initially are smaller in J20-PCSK9-MIX mice, recovered to match that of J20-  
40 AD mice later in the experimental protocol under normoxia (Figure 2D). Levels of oxyhaemoglobin

1 (HbO) were significantly reduced in PCSK9-ATH mice but showed a reduced trend in J20-PCSK9-MIX  
2 mice too. The washout of deoxyhaemoglobin (HbR) was significantly reduced in PCSK9-ATH mice  
3 compared to WT, but also showed a reduced trend across all diseased groups across all conditions  
4 compared to WT mice. All mice displayed stable and robust haemodynamic responses across the  
5 experimental protocol (Figure S2). Finally, vascular reactivity as determined by the response to 10%  
6 hypercapnia was not significantly different between any of the diseased groups (Figure S3).

7  
8 **CSD is Worse in Diseased Animals and Impacts Haemodynamic Recovery to Baseline**  
9 1-week after recovery from the chronic imaging protocol, an acute imaging experiment was performed  
10 wherein a small-burr hole was drilled into the skull overlying the active region (determined from HbT  
11 responses from chronic experiments) and a microelectrode was inserted into the brain to a depth of  
12 1500-1600 $\mu$ m to obtain neural electrophysiology data in combination with the imaging of cortical  
13 haemodynamics by 2D-OIS. Electrode insertion into the brain resulted in a wave of haemodynamic  
14 changes that occurred in all mice (CSD) (Figure 3). In WT mice, electrode insertion led to a small  
15 decrease in HbT (vasoconstriction) followed by a robust HbT bounce back (vasodilation), immediately  
16 followed by a small, sustained vasoconstriction (reduced HbT) that persisted for some time (Figure 3A-  
17 top). In J20-AD mice, electrode insertion caused a large vasoconstriction to occur which spread across  
18 the cortex in a strong wave of vasoconstriction that was followed by a very small, attempted recovery.  
19 This was masked by a large sustained and prolonged vasoconstriction of contiguous vessels that  
20 persisted for some time (Figure 3A-bottom). The largest vasoconstriction post-CSD occurred in J20-AD  
21 mice, followed by PCSK9-ATH mice, then J20-PCSK9-MIX mice compared to WT controls. The  
22 smallest of all CSD occurred in WT mice (Figure 3B). A prolonged and sustained constriction below  
23 baseline persisted in all mice post-CSD, however, this effect was recovered to baseline in WT mice  
24 during the first stimulation experiment 35 minutes after the CSD occurred (Figure 3B). In all disease  
25 mouse models, the constriction below baseline was more severe and persisted for a much longer time  
26 with a slower haemodynamic recovery. Following CSD, stimulation-evoked haemodynamic changes  
27 were not significantly different in any of the diseased groups overall, although they were initially smaller  
28 in the first two stimulations for PCSK9-ATH mice (Figure S1).

29  
30 **Stimulus-Evoked Neural Activity is Not Significantly Altered in Any Disease Groups Compared to WT**  
31 **Mice**

32 In the final imaging session and after a 35-minute period of recovery post-electrode insertion, the first  
33 experimental stimulation was performed (2s-stimulation in 100% oxygen) where evoked cortical  
34 haemodynamics were imaged simultaneously with the recording of neural multi-unit activity (MUA).  
35 Evoked-MUA response were not significantly different in any of the diseased groups compared to WT  
36 mice (Figure 4), suggesting that the significantly different evoked-HbT in PCSK9-ATH mice (observed  
37 on chronic imaging sessions) was due to neurovascular breakdown. Initially, the MUA was slightly lower  
38 for J20-AD, PCSK9-ATH & J20-PCSK9-MIX mice compared to WT mice (Figure 4A), however, later in  
39 the experimental session by the last stimulation, there was no observable difference in MUA between  
40 any of the groups (Figure 4D). Thus, this suggests that the neural MUA was initially smaller after the  
41 CSD had occurred, however, recovered fully with time. The haemodynamic responses in the acute

1 experimental session were not significantly different across all stimulations for any of the diseased  
2 groups.

3

4 Increased Number of Hippocampal A $\beta$  Plaques in J20-PCSK9-MIX Mice. Increased Neuroinflammation  
5 in J20-AD and PCSK9-ATH Mice

6 Immunohistochemistry was performed on J20-AD and J20-PCSK9-MIX mice to assess whether there  
7 were any specific differences in AD neuropathology changes. Staining was performed for A $\beta$  plaques  
8 and these were quantified within the hippocampus and the cortex. A $\beta$  plaques were significantly  
9 increased by 3-fold in the hippocampi of J20-PCSK9-MIX mice compared to J20-AD mice (Figure 5A/B).  
10 Within the cortex, there was no significant difference in A $\beta$  plaques between the 2 groups (data not  
11 shown). Next, neuroinflammation was assessed by qRT-PCR for 2 key inflammatory markers:  
12 interleukin-1 $\beta$  (IL1 $\beta$ ) and tumour necrosis factor- $\alpha$  (TNF $\alpha$ ) to assess the degree of neuroinflammation  
13 present globally within the brain. IL1 $\beta$  mRNA was significantly upregulated in J20-AD and PCSK9-ATH  
14 mice (Figure 5C). TNF $\alpha$  mRNA was significantly upregulated in PCSK9-ATH mice only (Figure 5D).  
15 J20-PCSK9-MIX mice displayed the lowest inflammatory changes in IL1 $\beta$  & TNF $\alpha$  compared to the  
16 other diseased groups, though this was still higher than WT mice.

17

18 **Discussion**

19 The present study investigated neurovascular function in a novel experimental model of atherosclerosis  
20 (PCSK9-ATH) and for the first time, in a comorbid setting whereby atherosclerosis was experimentally  
21 induced in a well characterised model of AD; J20-hAPP, to create a mixed comorbid model (J20-  
22 PCSK9-MIX). These mice were compared to age-matched (9-12m) WT C57BL/6J controls, and J20-  
23 AD mice. Given that systemic atherosclerosis is a major risk factor for dementia, the mechanisms  
24 underpinning the relationship between atherosclerosis, neurovascular decline and dementia are still  
25 largely unclear.

26

27 In the first part of the study, we characterised evoked-haemodynamic responses using a chronic skull-  
28 intact & surgery-recovered mouse preparation. We found that PCSK9-ATH mice displayed significantly  
29 reduced evoked blood volume (HbT) responses, in addition to reduced levels of oxyhaemoglobin (HbO)  
30 and notably, an impaired washout of deoxyhaemoglobin (HbR) across all stimulations and conditions.  
31 The J20-PCSK9-MIX mice did not display a significant reduction in HbT, nor in HbO or HbR levels. With  
32 respect to J20-AD mice, we did not observe any significant alterations to HbT as previously published  
33 (Sharp et al., 2019). Another important finding from the present study was that 10%-hypercapnia  
34 responses were not significantly different in any of the mice compared to WT controls (Figure S3), thus  
35 suggesting that vascular reactivity was not impaired in any of the mice, indicating that cerebral arterioles  
36 were unaffected by atherosclerosis at this time-point (9-12m). Thus, the basis of reduced HbT in  
37 PCSK9-ATH mice cannot be attributed to intracranial atherosclerosis. A recent study corroborated our  
38 findings showing that cerebrovascular reactivity and cerebral blood flow was preserved in the Tg-SwDI  
39 model of Alzheimer's (Munting et al., 2021), similar to our J20-model.

40

1 In the second part of the study, we obtained neural multi-unit activity (MUA) by inserting a multichannel  
2 electrode into the active region defined from the chronic imaging experiments. As we showed in our  
3 previous reports (Shabir et al., 2020; Sharp et al., 2019), the technical procedure of electrode insertion  
4 causes a cortical spreading depression (CSD) to occur in all animals. Here, we describe the CSD and  
5 its recovery on the different disease groups. CSD has two distinct phases: 1) a wave of depolarisation  
6 within the grey matter characterised by neuronal distortion leading to a large change of the membrane  
7 potential whereby neuronal activity is silenced (spreading depression) & 2) haemodynamic changes  
8 that accompany neuronal spreading depolarisation which typically result in a wave of prolonged  
9 reduced perfusion that persists for some time (Ayata & Lauritzen, 2015; Dreier, 2011). CSD does not  
10 typically occur in healthy brain tissue, however, it is a common neurophysiological occurrence in certain  
11 pathological conditions including migraine, epilepsy, brain injury, hyperthermia, hypoxia & ischaemia  
12 (Dreier, 2011). In WT mice, the initial constriction wave is small, and a robust haemodynamic recovery  
13 occurs which allows for neurovascular coupling to occur to sustain neurons metabolically. This is a  
14 marked difference to the diseased animals, which upon electrode insertion to cause a CSD, exhibit  
15 profound vasoconstriction with an extremely limited haemodynamic recovery resulting in a prolonged  
16 constriction, severe reductions to blood volume and HbO & HbR levels indicating hypoxia and  
17 ischaemia. Thus, the haemodynamic response to CSD in diseased mice is severely inappropriate and  
18 can lead to long lasting devastating effects such as widespread cortical pannecrosis of neurons and  
19 astrocytes (Dreier, 2011). As our data show, baseline blood volumes do not recover in the diseased  
20 animals for a much longer period compared to WT animals, with the most profound CSD occurring in  
21 J20-AD mice, followed by PCSK9-ATH mice.

22  
23 CSD may be the neuropathological link between migraine, stroke, cardiovascular disease and dementia  
24 in which cardiovascular risk factors, genetics and other lifestyle factors which prime the onset of  
25 migraine to occur lead to vascular vulnerability within the brain predisposing affected individuals to an  
26 increased risk of cerebral ischaemia and haemorrhagic stroke (Ripa et al., 2015). There is accumulating  
27 evidence to suggest that shared genetic and associated clinical features observed in migraine patients  
28 are involved in the increased vulnerability to cerebral ischaemia, therefore, predisposing affected  
29 individuals to stroke and white matter lesions associated with dementia (Yemisci & Eikermann-Haerter,  
30 2019). The underlying mechanism being CSD; the neurophysiological feature of aura in migraines,  
31 whose induction threshold can be reduced by genetic mutations and systemic comorbidities that  
32 contribute to vascular dysfunction and neuroinflammation (Yemisci & Eikermann-Haerter, 2019).  
33 Indeed, mouse models of cerebral autosomal dominant arteriopathy with subcortical infarcts and  
34 leukoencephalopathy syndrome (CADASIL); a genetic cerebrovascular disease caused by *NOTCH3*  
35 mutations that has a high frequency of migraines with aura, have enhanced CSD linking a dysfunctional  
36 neurovascular unit with migraine with aura (Eikermann-Haerter et al., 2011). Furthermore, a recent  
37 study examined women who suffered from migraines with and without aura and found that those that  
38 suffered migraines with aura had a higher incidence rate of cardiovascular disease compared to women  
39 without aura or any migraines (Kurth et al., 2020). In addition, another recent study found that migraine  
40 history was positively associated with an increased risk of developing both all-cause dementia and AD,

1 but not VaD (Morton et al., 2019). Our study, along with the previously discussed studies provide an  
2 explanation for these recent findings and highlights how systemic disease can prime the brain to allow  
3 profound CSDs to occur in the context of migraine, and as such, migraine frequency and intensity may  
4 be related to the onset of neurological disease by later in life including dementia.

5  
6 Neural MUA data was not significantly altered across any of the stimulations or conditions for any of  
7 the disease groups compared to WT controls. A consistent finding irrespective of stimulation and  
8 condition was that PCSK9-ATH mice display consistently reduced evoked-HbT responses (observed in  
9 chronic experiments) compared to WT controls, which suggests an advanced level of neurovascular  
10 breakdown and inefficiency. Other groups have found similarly reduced blood flow in the ApoE<sup>-/-</sup> model  
11 without altered cortical activation (Ayata et al., 2013). A recent study found decreased tissue  
12 oxygenation in the LDLR<sup>-/-</sup> mouse model of atherosclerosis (Li et al., 2019), and this is most likely to be  
13 the case in the PCSK9 model.

14  
15 A question that arises is why the J20-PCSK9-MIX mice HbT responses are not more severely impaired  
16 than J20-AD and PCSK9-ATH? There may be redundancies that occur physiologically to compensate  
17 for mild hypoxia in the brain, such as the possible angiogenesis within the brain. Angiogenesis is known  
18 to be triggered in cerebral microvessels in AD in response to increased A $\beta$  and neuroinflammation and  
19 may initially reflect a compensatory mechanism to increase perfusion (Jefferies et al., 2013). In addition,  
20 the levels of neuroinflammation seen in these mice may be due to an altered disease-course and  
21 examining temporospatial expression may reveal much higher levels of inflammation in this mixed  
22 model at an earlier time-point. Other markers of inflammation may be upregulated compared to those  
23 that we assessed, and future studies would incorporate transcriptomic approaches to identify other  
24 mechanisms or markers. Nevertheless, a key translational finding from our study was that J20-PCSK9-  
25 MIX mice displayed a significant increase in the number of hippocampal plaques.

26  
27 There are several notable limitations with the present study. Firstly, all imaging was performed on lightly  
28 anaesthetised animals, which is known to compromise neurovascular function (Gao et al., 2017).  
29 However, previous research from our laboratory has developed an anaesthetic regimen that is  
30 comparable to awake imaging in terms of the haemodynamic responses to physiological whisker  
31 stimulation with little effect on vascular reactivity (Sharp et al., 2015). The benefits of lightly  
32 anaesthetised preparations over awake preparations is that we can avoid the multiple considerations  
33 of behavioural state in which the animals may be whisking, grooming as well as their arousal and stress  
34 states which may be present in awake animals. Furthermore, we report the stability and robustness of  
35 our imaging preparation in this study. We present the average of all the raw stimulation trials from each  
36 animal across the whole experimental session (Figure S2), showing the stability and robustness of our  
37 preparation, as well as easily identifying any changes. Secondly, our imaging analysis assumes O<sub>2</sub>  
38 saturation to be 70% with a baseline haemoglobin concentration of 100 $\mu$ M. This may be important if  
39 the assumed baselines are different in the diseased animals compared to WT controls; however, our  
40 recent study (Sharp et al., 2019) using the same J20-AD mouse model discussed this issue in detail,

1 in which we showed that regardless of the baseline blood volume estimation used, our percentage  
2 change was scaled by it (i.e. always the same change). Therefore, the observations in this paper with  
3 respect to the different diseased animals are robust.

4

5 In conclusion, we report novel findings of impaired neurovascular function in a novel experimental  
6 model of atherosclerosis (PCSK9-ATH) characterised by reduced stimulus-evoked blood volume  
7 without any significant alterations to evoked neural activity. We induced atherosclerosis in a mild fAD  
8 model (J20-AD) to create a mixed comorbid model (J20-PCSK9-ATH) in which we report a significant  
9 increase in the number of hippocampal A $\beta$  plaques, however, without any significant changes to evoked  
10 haemodynamic or neural responses compared to WT or J20-AD mice. A key finding from this study  
11 was CSD was more severe in diseased animals. This may reflect the global inflammatory state of the  
12 brain and could also serve to be an effective preclinical and human clinical biomarker for baseline state  
13 and to assess therapies. Future studies should include assessment of other inflammatory markers and  
14 cellular pathway changes by a genome wide transcriptomics approach from single cell populations. It  
15 would also be prudent to induce atherosclerosis in a more severe fAD model to provide a severity  
16 continuum of mixed models that reflect clinical presentations of dementia.

17

## 18 **Materials & Methods**

### 19 Animals

20 All animal procedures were performed with approval from the UK Home Office in accordance to the  
21 guidelines and regulations of the Animal (Scientific Procedures) Act 1986 and were approved by the  
22 University of Sheffield ethical review and licensing committee. Male C57BL/6J mice were injected i.v at  
23 6wks with 6x10<sup>12</sup> virus molecules/ml rAAV8-mPCSK9-D377Y (Vector Core, Chapel Hill, NC) and fed a  
24 Western diet (21% fat, 0.15% cholesterol, 0.03% cholate, 0.296% sodium; #829100, Special Diet  
25 Services UK) for 8m (PCSK9-ATH). These mice were compared to age-matched wild-type C57BL/6J  
26 mice (with no AAV injection fed normal rodent chow) that were used as controls (WT C57BL/6J). In  
27 addition, male heterozygous transgenic J20-hAPP B6.Cg-Zbtb20Tg(PDGFB-  
28 APPSwInd)20Lms/2Mmjx (MMRRC Stock No: 34836-JAX) mice were used. Atherosclerosis was  
29 induced in J20-hAPP mice alongside WT mice at 6wks of age combined with a Western diet to create  
30 a comorbid mixed model (J20-PCSK9-MIX). For the CSD imaging experiments, 4 nNOS-ChR2 mice  
31 (M/F, 16-40 weeks old) were included in the WT group. [nNOS-ChR2 mice: heterozygous nNOS-CreER  
32 (Jax 014541, (Taniguchi et al., 2011)) x homozygous Ai32 mice (Jax 024109, (Madisen et al., 2012)),  
33 given tamoxifen (100mg/kg, i.p., 3 injections over 5 days) at 1-2 months old]. All mice were imaged  
34 between 9-12m of age. All mice were housed in a 12hr dark/light cycle at a temperature of 23C, with  
35 food and water supplied *ad-libitum*.

36

### 37 Thinned Cranial Window Surgery

38 Mice were anaesthetised with 7ml/kg i.p. injection of fentanyl-fluanisone (Hypnorm, Vetapharm Ltd),  
39 midazolam (Hypnovel, Roche Ltd) and maintained in a surgical anaesthetic plane by inhalation of  
40 isoflurane (0.6-0.8% in 1L/min O<sub>2</sub>). Core body temperature was maintained at 37°C through use of a

1 homeothermic blanket (Harvard Apparatus) and rectal temperature monitoring. Mice were placed in a  
2 stereotaxic frame (Kopf Instruments, US) and the bone overlying the right somatosensory cortex was  
3 thinned forming a thinned cranial optical window. A thin layer of clear cyanoacrylate glue was applied  
4 over the cranial window to reinforce the window. Dental cement was applied around the window to  
5 which a metal head-plate was chronically attached. All mice were given 3 weeks to recover before the  
6 first imaging session.

7

8 2D-Optical Imaging Spectroscopy (2D-OIS)

9 2D-OIS measures changes in cortical haemodynamics: total haemoglobin (HbT), oxyhaemoglobin  
10 (HbO) and deoxyhaemoglobin (HbR) concentrations (Berwick et al., 2005). Mice were lightly sedated  
11 and placed into a stereotaxic frame. Sedation was induced as described above and maintained using  
12 low levels of isoflurane (0.3-0.6%). For imaging, the right somatosensory cortex was illuminated using  
13 4 different wavelengths of light appropriate to the absorption profiles of the differing haemoglobin states  
14 (495nm ± 31, 559nm ± 16, 575nm ± 14 & 587nm ± 9) using a Lambda DG-4 high-speed galvanometer  
15 (Sutter Instrument Company, US). A Dalsa 1M60 CCD camera was used to capture the re-emitted light  
16 from the cortical surface. All spatial images recorded from the re-emitted light underwent spectral  
17 analysis based on the path length scaling algorithm (PLSA) as described previously (Berwick et al.,  
18 2005; Mayhew et al., 1999). which uses a modified Beer-Lambert law with a path light correction factor  
19 converting detected attenuation from the re-emitted light with a predicted absorption value. Relative  
20 HbT, HbR and HbO concentration estimates were generated from baseline values in which the  
21 concentration of haemoglobin in the tissue was assumed to be 100µM and O<sub>2</sub> saturation to be 70%.  
22 For the stimulation experiments, whiskers were mechanically deflected for a 2s-duration and a 16s-  
23 duration at 5Hz using a plastic T-shaped stimulator which caused a 1cm deflection of the left-whisker.  
24 Each individual experiment consisted of 30 stimulation trials (for 2s) and 15 stimulation trials (for 16s)  
25 of which a mean trial was generated after spectral analysis of 2D-OIS. Stimulations were performed  
26 with the mouse breathing in 100% O<sub>2</sub> or 21% O<sub>2</sub>, and a gas transition to medical air (21% O<sub>2</sub>) as well  
27 as an additional 10% CO<sub>2</sub>-hypercapnia test of vascular reactivity.

28

29 Neural Electrophysiology

30 Simultaneous measures of neural activity alongside 2D-OIS were performed in a final acute imaging  
31 session 1-week after the 1st imaging session. A small burr-hole was drilled through the skull overlying  
32 the active region (as defined by the biggest HbT changes from 2D-OIS imaging) and a 16-channel  
33 microelectrode (100µm spacing, 1.5-2.7MΩ impedance, site area 177µm<sup>2</sup>) (NeuroNexus Technologies,  
34 USA) was inserted into the whisker barrel cortex to a depth of ~1500µm. The microelectrode was  
35 connected to a TDT preamplifier and a TDT data acquisition device (Medusa BioAmp/RZ5, TDT, USA).  
36 Multi-unit analysis (MUA) was performed on the data. All channels were depth aligned to ensure we  
37 had twelve electrodes covering the depth of the cortex in each animal. The data were high passed  
38 filtered above 300Hz to remove all low frequency components and split into 100ms temporal bins. Within  
39 each bin any data crossing a threshold of 1.5SD above the mean baseline was counted and the results  
40 presented in the form of fractional changes to MUA.

1

2 Region Analysis

3 Analysis was performed using MATLAB (MathWorks). An automated region of interest (ROI) was  
4 selected using the stimulation data from spatial maps generated using 2D-OIS. The threshold for a pixel  
5 to be included within the ROI was set at 1.5xSD, therefore the automated ROI for each session per  
6 animal represents the area of the cortex with the largest haemodynamic response, as determined by  
7 the HbT. For each experiment, the response across all pixels within the ROI was averaged and used  
8 to generate a time-series of the haemodynamic response against time.

9

10 Statistical Analysis

11 Statistical analyses were performed using SPSS v25 & GraphPad Prism v8. Shapiro-Wilks test was  
12 used to check for normality and Levene's test was used to assess equality of variances. 2-way mixed  
13 design ANOVA, 1-way ANOVA or Kruskal-Wallis tests were used, as appropriate. For 1-way ANOVA,  
14 if variances were unequal, Welch's F was reported. Results were considered statistically significant if  
15  $p < 0.05$ . The Shapiro-Wilks test suggested that, for chronic experiments, peak values of HbT and HbO  
16 are normally distributed, however, HbR values are significantly non-normal. 2-way mixed design was  
17 used to compare peak values for HbT, HbO & HbR (although HbR failed the S-W test for normality, an  
18 ANOVA was used as they were considered fairly robust against small deviations from normality).  
19 Inspection of Levene's test suggested that variances were equal, therefore, Dunnett's (two-sided)  
20 multiple comparisons test was used to compare disease models to WT, and for HbR, Games-Howell  
21 multiples comparisons were used. If the Greenhouse-Geisser estimate of sphericity showed deviation  
22 from sphericity (chronic experiments: HbT ( $\epsilon = 0.55$ ), HbO ( $\epsilon = 0.49$ ) & HbR ( $\epsilon = 0.564$ ), results are  
23 reported with Greenhouse-Geisser correction applied. qRT-PCR data was analysed by performing 1-  
24 way ANOVAs with Dunnett's multiple comparisons test used to compare disease models to WT. P-  
25 values  $< 0.05$  were considered statistically significant. All the data are presented as mean values  $\pm$   
26 standard error of mean (SEM).

27

28 Immunohistochemistry

29 At the end of terminal experiments, mice were euthanized with an overdose of pentobarbital (100mg/kg,  
30 Euthatal, Merial Animal Health Ltd) and transcardially perfused with 0.9% saline and brains were  
31 dissected. One half-hemisphere of the brains were fixed in formalin and embedded in paraffin wax, with  
32 the other half snap-frozen using isopentane and stored at -80C. 5 $\mu$ m coronal sections were obtained  
33 using a cryostat. Immunohistochemistry was performed using an avidin-biotin complex (ABC) method  
34 (as described previously (Ameen-Ali et al., 2019)). Following slide preparation and antigen retrieval  
35 (pressure cooker at 20psi at 120C for 45s (pH6.5)), sections underwent additional pre-treatment in 70%  
36 formic acid. Sections were incubated with 1.5% normal serum followed by incubation with the primary  
37 antibody (biotinylated anti-A $\beta$  – 1:100, BioLegend, USA) for 1 hour. Horseradish peroxidase avidin-  
38 biotin complex (Vectastain Elite Kit, Vector Laboratories, UK) was used to visualise antibody binding  
39 along with 3,3-diaminobenzidine tetrahydrochloride (DAB) (Vector Laboratories, UK). All sections were  
40 counterstained with haematoxylin, dehydrated and mounted in DPX. Sections were imaged using a

1 Nikon Eclipse Ni-U microscope attached to a Nikon DS-Ri1 camera. Plaques were identified at x40  
2 magnification and manually counted per section.

3

4 qRT-PCR

5 Snap-frozen hemispheres were homogenised, and RNA was extracted using Direct-zol RNA MiniPrep  
6 kit with TRI-reagent as per the manufacturer's guidelines (Zymo) and RNA quality checked using  
7 NanoDropTM (ThermoFisher Scientific). cDNA was synthesised from the extracted RNA using the  
8 UltraScript 2.0 cDNA synthesis kit (PCR BioSystems) according to the manufacturer's guidelines. qRT-  
9 PCR was performed using PrimeTime qRT-PCR assay primers (IDT) for *IL1 $\beta$*  & *TNF $\alpha$*  with *ACTB* as  
10 the reference housekeeping gene. Luna qRT-PCR Master Mix (NEB) was used with the primers, cDNA  
11 and nuclease free water and each gene for each sample was duplicated. CFX384 Real-Time System  
12 (BioRad) with a C1000 Touch Thermal Cycler (BioRad) was used to perform qRT-PCR consisting of 40  
13 cycles. Data was analysed using the well-established delta-Ct method (Livak & Schmittgen, 2001) by  
14 normalising against *ACTB*.

15

16

17

18

19

20

21

22

23

24

25

26

27

28

29

30

31

32

33

34

35

36

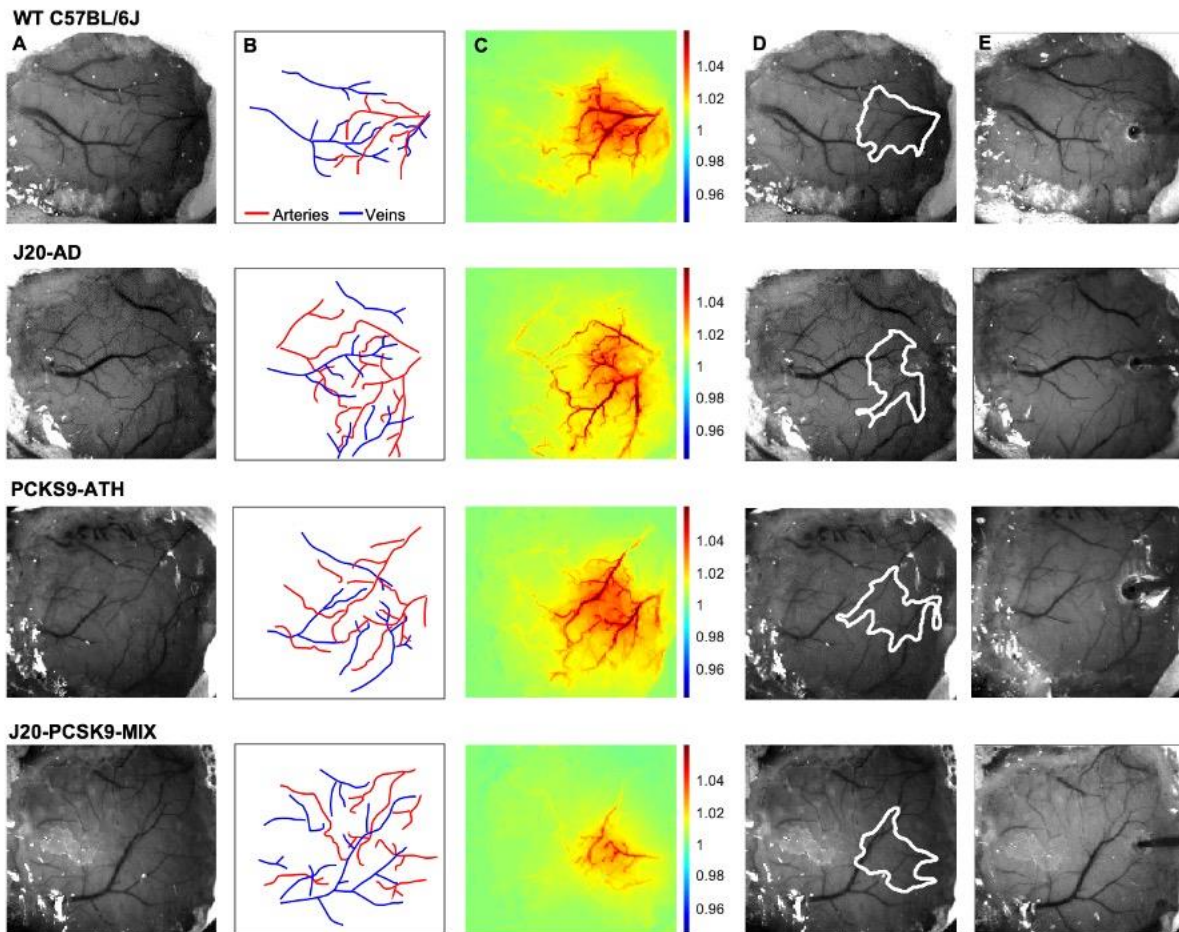
37

38

39

40

## 1 Figures



2

3 **Figure 1: Experimental Setup and Data Derivation.** **A)** Raw image of representative thinned cranial  
4 windows for WT, J20-AD, PCKS9-ATH AND J20-PCSK9-MIX mice (chronic imaging session). **B)**  
5 Vessel map outlining the major arteries and veins within the thinned cranial window. **C)** HbT spatial  
6 activation map showing fractional changes in HbT in response to a 16s-whisker stimulation. **D)**  
7 Automated computer-generated region of interest (ROI) determined from the HbT activation response  
8 in C from which time-series for HbT, HbO & HbR are generated. **E)** Raw image of the same animals in  
9 terminal acute imaging sessions with multichannel electrodes inserted into the active ROI determined  
10 from chronic imaging session.

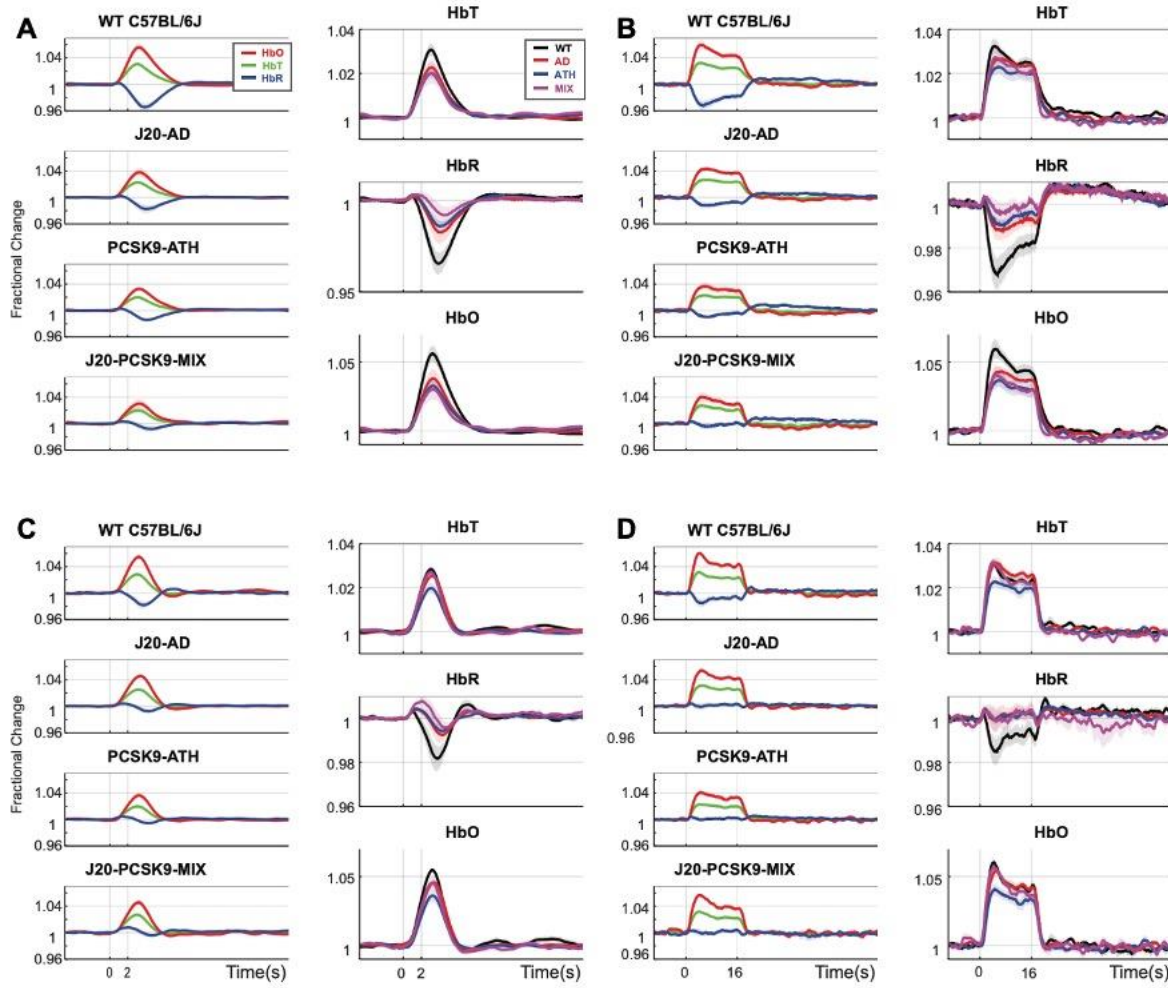


**Figure 2: Fractional Changes in Chronic Stimulus-Evoked (Peak) Haemodynamic Responses. A)**

2s-stimulation in 100% oxygen. **B)** 16s-stimulation in 100% oxygen. **C)** 2s-stimulation in 21% oxygen.

**D)** 16s-stimulation in 21% oxygen. All animals aged 9-12m: WT (n=6), J20-AD (n=9), PCSK9-ATH

(n=8), J20-PCSK9-MIX (n=6). **HbT:** There was no significant overall effect of disease  $F(3,25)=2.83$ ,

$p=0.059$ . However, Dunnett's (two-sided) multiple comparisons test revealed there was a significant

difference between WT and ATH ( $p=0.023$ ). As expected, there was a significant effect of experiment,

$F(1.65,41.14)=13.64$ ,  $p<0.001$ . There was also no significant interaction effect between experiment and

disease,  $F(4.94,41.14)=1.50$ ,  $p=0.211$ . **HbO:** There was a significant overall effect of disease

$F(3,25)=4.84$ ,  $p=0.009$ . Dunnett's (two-sided) multiple comparisons test revealed there was a significant

difference between WT and ATH ( $p=0.002$ ). There was a significant effect of experiment,

$F(1.47,36.72)=15.348$ ,  $p<0.001$ . There was no significant interaction effect between experiment and

disease,  $F(4.41,36.72)=1.64$ ,  $p=0.181$ . **HbR:** There was a significant overall effect of disease

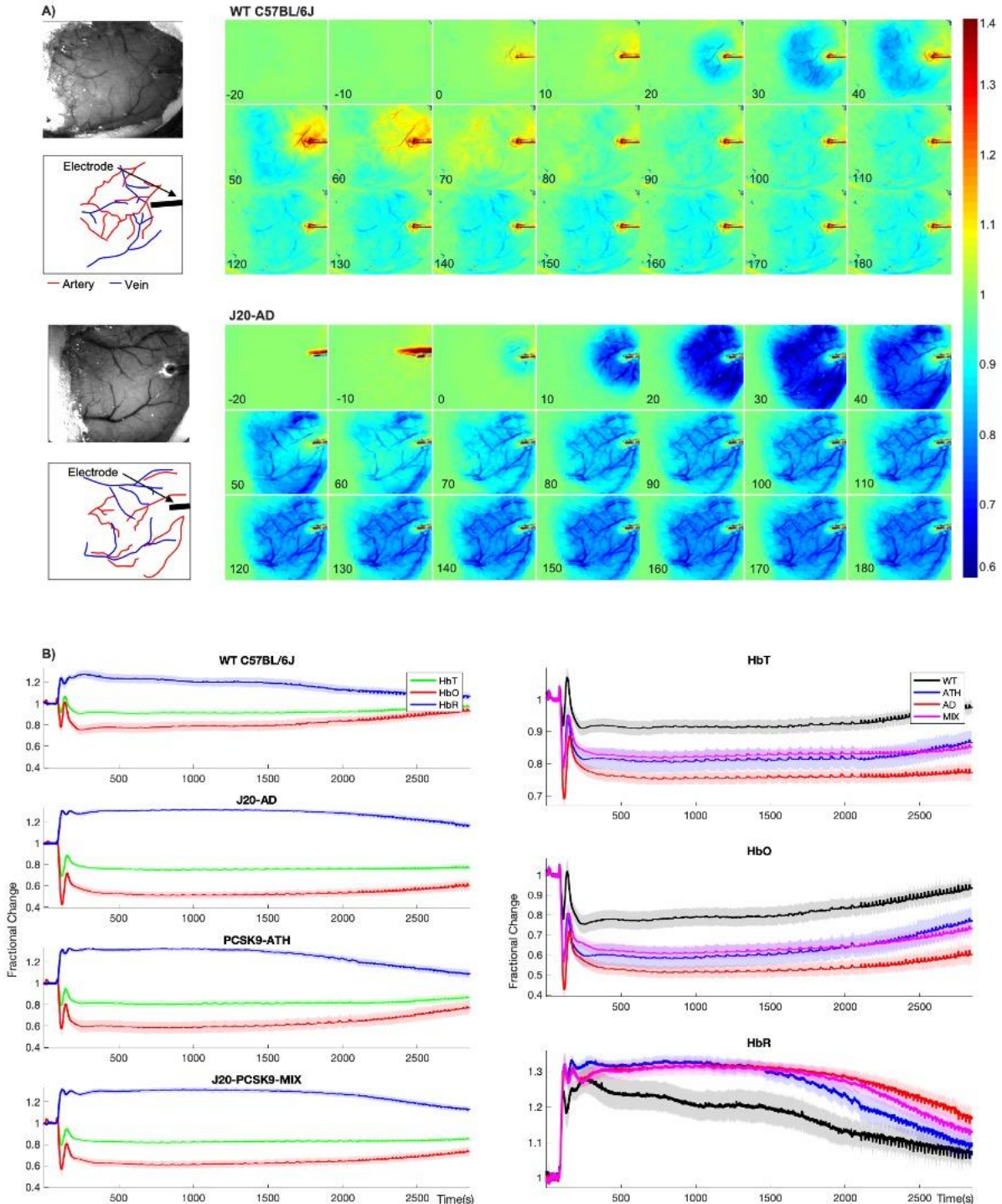
$F(3,25)=4.86$ ,  $p=0.008$ . Games-Howell multiple comparisons reveal HbR peak is significantly different

for WT vs ATH ( $p=0.040$ ). There was a significant effect of experiment,  $F(1.69,42.28)=17.33$ ,  $p<0.001$ .

There was a significant interaction between experiment and disease interaction:  $F(5.07, 42.28)=3.19$ ,

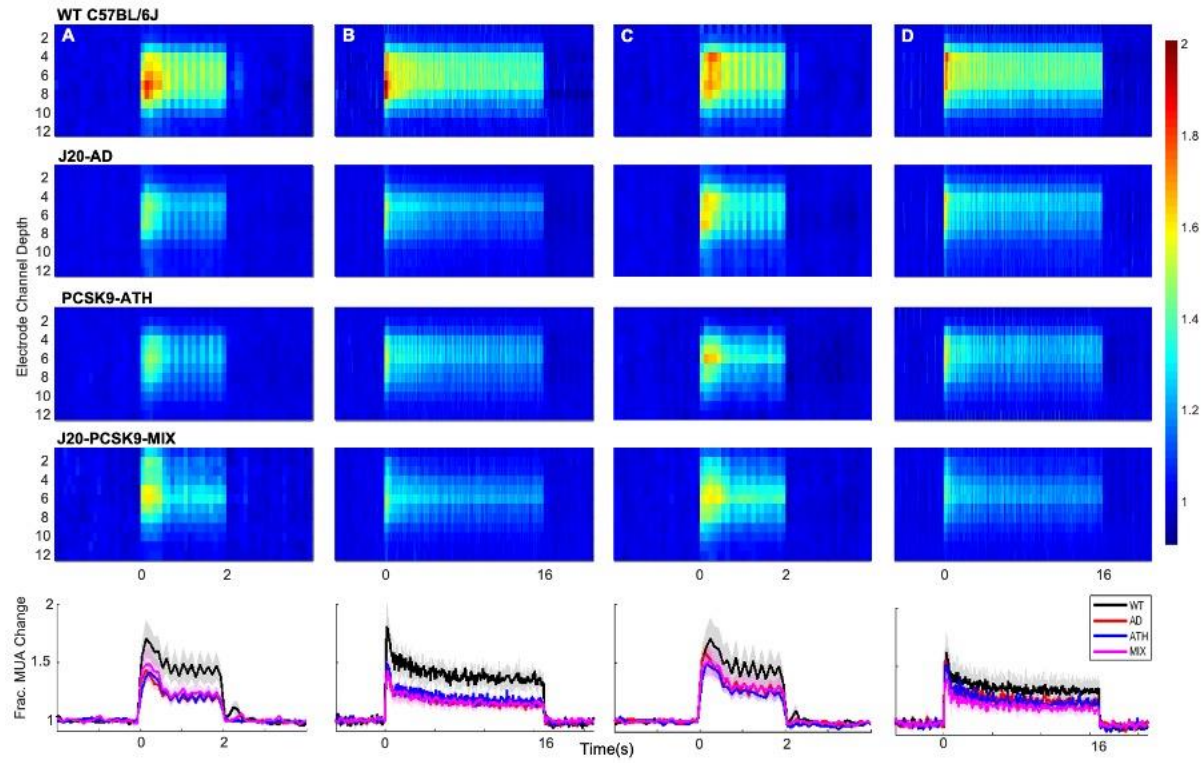
$p=0.015$ . All error bars (lightly shaded) are  $\pm$ SEM. Vertical dotted lines indicate start and end of

stimulations.

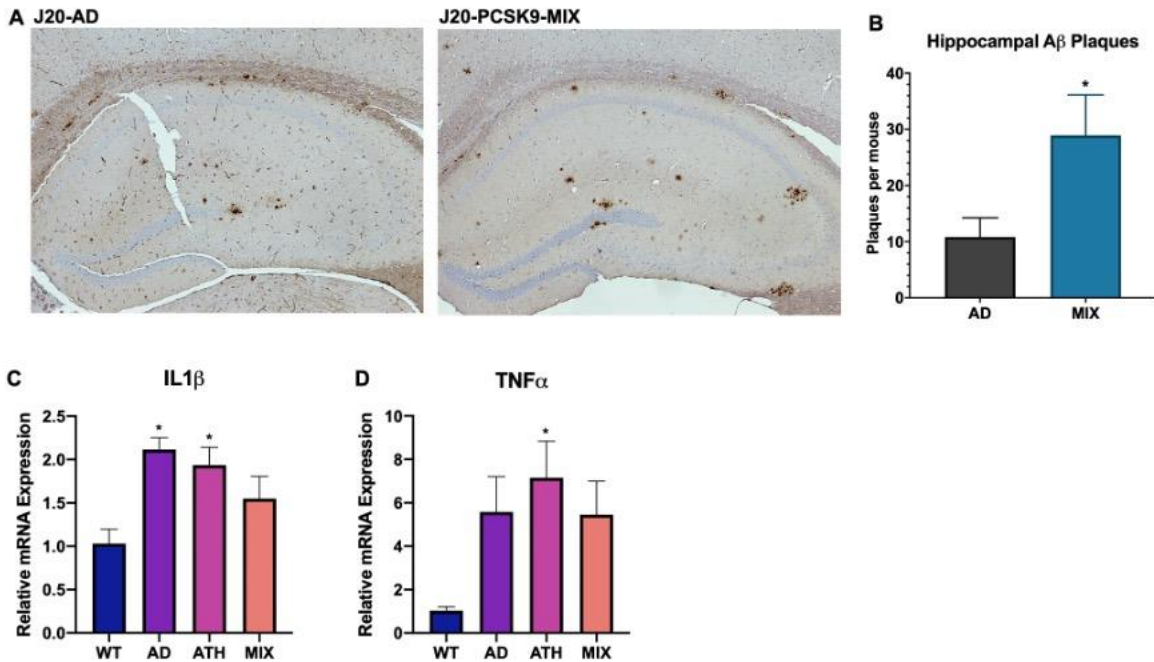


1  
2 **Figure 3: Cortical Spreading Depression (CSD) in WT, diseased and comorbid animals. A)**  
3 Representative montage time-series of WT and J20-AD mice showing HbT changes post-electrode  
4 insertion. Colour bar represents fractional changes in HbT from baseline. **B)** *Left:* Average CSD  
5 haemodynamics profiles for control animals (WT C57BL/6J & nNOS-ChR2) (n=7), J20-AD (n=7),  
6 PCSK9-ATH (n=5) & J20-PCSK9-MIX (n=6) mice. *Right:* Averaged changes to HbT (top), HbO (middle)  
7 & HbR (bottom) upon CSD in the different mouse groups compared to WT. **HbT:** A 1-way ANOVA  
8 showed significant effect of disease for HbT ( $F(3,21)=9.62$ ,  $p=0.001$ ). Dunnett's 2-sided multiple

1 comparisons showed that AD vs WT  $p<0.001$ , ATH vs WT  $p=0.012$  & MIX vs WT  $p=0.020$ . **HbO:** 1-way  
2 ANOVA showed significant effect of disease for HbO ( $F(3,21)=8.51$ ,  $p<0.001$ ). Dunnett's 2-sided multiple  
3 comparisons showed that AD vs WT  $p<0.001$ , ATH vs WT  $p=0.01$  & MIX vs WT  $p=0.017$ . **HbR:** Kruskal-  
4 Wallis test revealed no significant effect of disease  $H(3)=6.58$ ,  $p=0.087$ . All error bars (lightly shaded)  
5 are  $\pm$ SEM.  
6  
7  
8  
9  
10  
11  
12  
13  
14  
15  
16  
17  
18  
19  
20  
21  
22  
23  
24

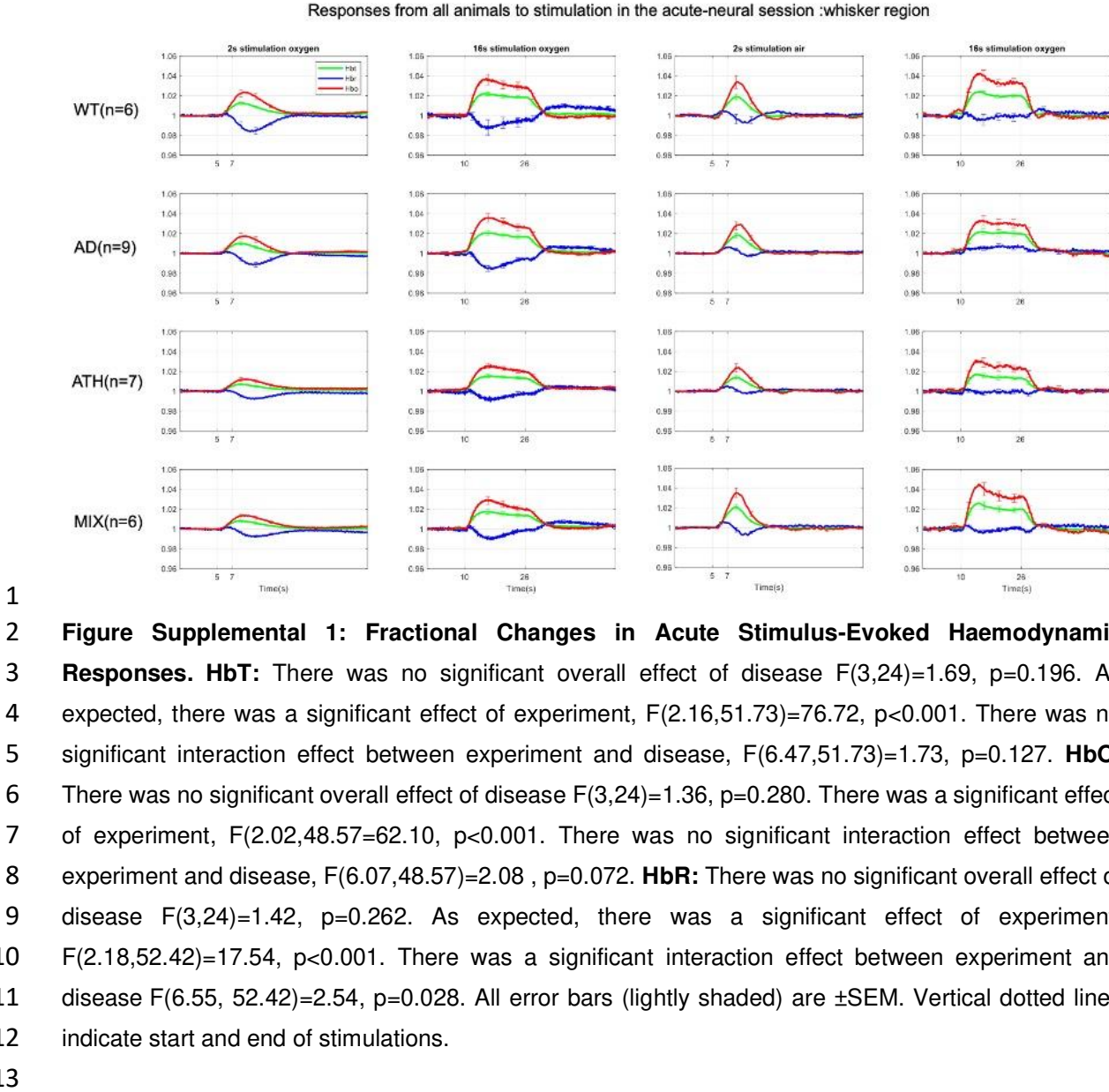


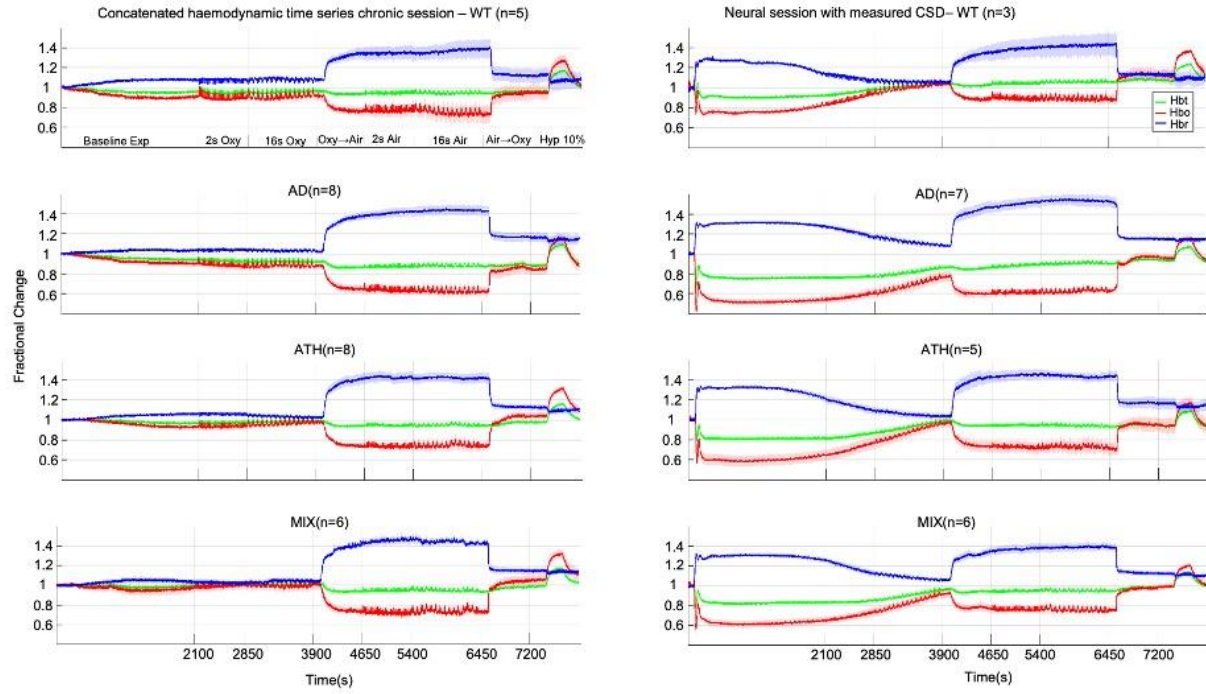
1  
2 **Figure 4: Evoked Neural Multi-Unit Activity (MUA) Responses.** MUA heat maps showing fractional  
3 changes in MUA along the depth of the cortex (channels 4-8) in response to stimulations in WT  
4 C57BL/6J (n=6), J20-AD (n=9), PCSK9-ATH (n=7) & J20-PCSK9-MIX (n=6) mice. Overall effect of  
5 disease on MUA  $F(3,24)=2.24$ ,  $p=0.109$  (2-way mixed design ANOVA). There was a significant effect  
6 of experiment, as expected,  $F(2.26, 54.16)=6.83$ ,  $p=0.002$ . There was no significant interaction between  
7 experiment and disease  $F(6.77, 54.16)=0.70$ ,  $p=0.670$ . All error bars (lightly shaded) are  $\pm$ SEM.  
8  
9  
10



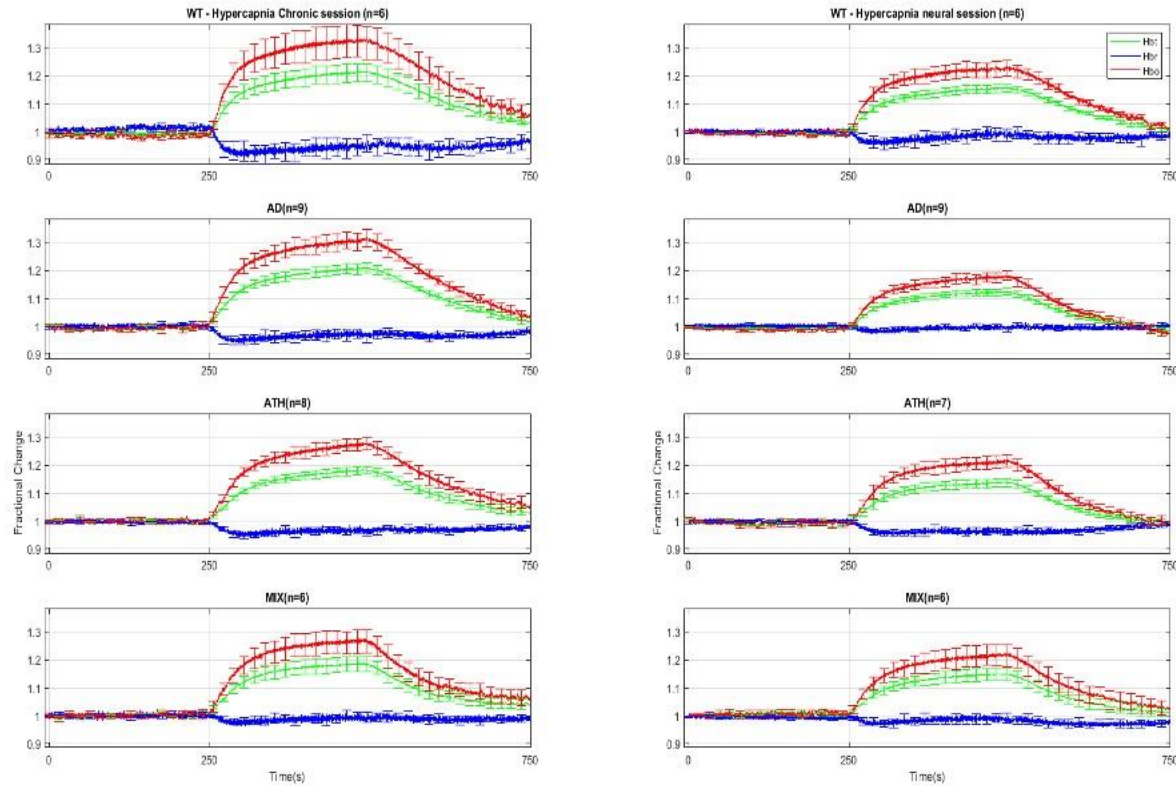
**Figure 5: Neuropathology and Neuroinflammation.** A) Representative histological coronal hippocampal sections for J20-AD and J20-PCSK9-MIX mice stained with anti-A $\beta$  to visualise A $\beta$  plaques. B) Increased number of amyloid-beta plaques in the hippocampus of J20-PCSK9-MIX mice compared to J20-AD mice ( $p=0.036$ ; unpaired t-test) ( $n=4$  each). Cortical plaques  $p=0.3372$  (data not shown). C) qRT-PCR for IL1 $\beta$ : AD vs WT  $p=0.011$ , ATH vs WT  $p=0.0278$ , MIX vs WT  $p=0.218$  (1-way ANOVA with post-hoc Dunnett's multiple comparisons test). D) qRT-PCR for TNF $\alpha$ : AD vs WT  $p=0.1197$ , ATH vs WT  $p=0.0370$ , MIX vs WT  $p=0.1313$  with post-hoc Dunnett's multiple comparisons test. All error bars are  $\pm$ SEM.

10  
11  
12





1  
2 **Figure Supplemental 2: Concatenated data showing stability and robustness of the mouse**  
3 **imaging preparation.** Left) Chronic imaging sessions including a 35-minute haemodynamics baseline  
4 before first stimulation. Right) Acute imaging sessions including CSD plus 35-minute haemodynamics  
5 recovery before first stimulation.  
6  
7  
8  
9



1  
2 **Figure Supplemental 3: Chronic (Left) & Acute (Right) Hypercapnia.** Chronic: A 1-way ANOVA  
3 showed no significant effect of disease for HbT ( $F(3,12.06)=0.49$ ,  $p=0.694$ ), HbO ( $F(3,11.98)=0.44$ ,  
4  $p=0.732$ ) nor HbR ( $F(3,12.081)=0.98$ ,  $p=0.436$ ). Acute: A 1-way ANOVA showed no significant effect  
5 of disease for HbO  $F(3,12.00)=0.74$ ,  $p=0.549$  but there was a significant effect of disease for HbR  
6  $F(3,11.01)=3.77$ ,  $p=0.044$ . Games-Howell multiple comparisons showed that, for HbR, there was a  
7 significant difference between AD and ATH ( $p=0.019$ ). Kruskal-Wallis test showed no significant effect  
8 of disease for HbT:  $H(3)=2.87$ ,  $p=0.412$ . Error bars  $\pm$ SEM.

9  
10  
11  
12  
13  
14  
15  
16  
17  
18  
19  
20  
21  
22  
23  
24

1 **Acknowledgments**

2 OS's PhD studentship and consumables were funded by the Neuroimaging in Cardiovascular Disease  
3 (NICAD) network scholarship (University of Sheffield). A British Heart Foundation (BHF) project grant  
4 was awarded to SEF to carry out the work using the PCSK9 model (PG/13/55/30365). The J20-mouse  
5 colony was in part funded and supported by Alzheimer's Research UK (Grant R/153749-12-1). CH is  
6 funded by a Sir Henry Dale Fellowship jointly funded by the Wellcome Trust and the Royal Society.  
7 This research was funded in whole, or in part, by the Wellcome Trust [Grant number 105586/Z/14/Z].  
8 For the purpose of Open Access, the author has applied a CC BY public copyright licence to any Author  
9 Accepted Manuscript version arising from this submission. MAR is funded by a Conacyt scholarship.  
10 We would like to thank Prof Lennart Mucke (Gladstone Institute of Neurological Disease & Department  
11 of Neurology, UCSF, CA, US) as well as the J. David Gladstone Institutes for the J20-hAPP mice.  
12 Finally, we would like to thank Mr Michael Port for building and maintaining the imaging apparatus and  
13 Dr Luke Boorman for producing MATLAB code for data analysis.

14

15 **Conflicts of Interest**

16 The authors have no conflicts of interests to declare.

17

18 **Author Contributions**

19 OS performed the majority of the *in vivo* experiments and authored the manuscript. OS & JB designed  
20 the experiments. OS, BP, LL, BE, PS & MAR performed experiments. OS, CH & JB performed MATLAB  
21 and data analysis. JB, SEF, CH, PRH & SBW supervised the research and provided editorial guidance.  
22 All authors proofread the final version of the manuscript.

23

24 **References**

25 Ameen-Ali, K. E., Simpson, J. E., Wharton, S. B., Heath, P. R., Sharp, P. S., Brezzo, G., & Berwick, J.  
26 (2019). The Time Course of Recognition Memory Impairment and Glial Pathology in the hAPP-  
27 J20 Mouse Model of Alzheimer's Disease. *J Alzheimers Dis*, 68(2), 609-624.  
28 <https://doi.org/10.3233/JAD-181238>

29 Ayata, C., & Lauritzen, M. (2015). Spreading Depression, Spreading Depolarizations, and the Cerebral  
30 Vasculature. *Physiol Rev*, 95(3), 953-993. <https://doi.org/10.1152/physrev.00027.2014>

31 Ayata, C., Shin, H. K., Dilekoz, E., Atochin, D. N., Kashiwagi, S., Eikermann-Haerter, K., & Huang, P.  
32 L. (2013). Hyperlipidemia disrupts cerebrovascular reflexes and worsens ischemic perfusion  
33 defect. *J Cereb Blood Flow Metab*, 33(6), 954-962. <https://doi.org/10.1038/jcbfm.2013.38>

34 Berwick, J., Johnston, D., Jones, M., Martindale, J., Redgrave, P., McLoughlin, N., Schiessl, I., &  
35 Mayhew, J. E. (2005). Neurovascular coupling investigated with two-dimensional optical  
36 imaging spectroscopy in rat whisker barrel cortex. *Eur J Neurosci*, 22(7), 1655-1666.  
37 <https://doi.org/10.1111/j.1460-9568.2005.04347.x>

38 Bjorklund, M. M., Hollensen, A. K., Hagensen, M. K., Dagnaes-Hansen, F., Christoffersen, C.,  
39 Mikkelsen, J. G., & Bentzon, J. F. (2014). Induction of atherosclerosis in mice and hamsters  
40 without germline genetic engineering. *Circ Res*, 114(11), 1684-1689.  
41 <https://doi.org/10.1161/CIRCRESAHA.114.302937>

42 Dreier, J. P. (2011). The role of spreading depression, spreading depolarization and spreading ischemia  
43 in neurological disease. *Nat Med*, 17(4), 439-447. <https://doi.org/10.1038/nm.2333>

44 Eikermann-Haerter, K., Yuzawa, I., Dilekoz, E., Joutel, A., Moskowitz, M. A., & Ayata, C. (2011).  
45 Cerebral autosomal dominant arteriopathy with subcortical infarcts and leukoencephalopathy  
46 syndrome mutations increase susceptibility to spreading depression. *Ann Neurol*, 69(2), 413-  
47 418. <https://doi.org/10.1002/ana.22281>

1 Gao, Y. R., Ma, Y., Zhang, Q., Winder, A. T., Liang, Z., Antinori, L., Drew, P. J., & Zhang, N. (2017).  
2 Time to wake up: Studying neurovascular coupling and brain-wide circuit function in the un-  
3 anesthetized animal. *Neuroimage*, 153, 382-398.  
4 <https://doi.org/10.1016/j.neuroimage.2016.11.069>

5 Iadecola, C. (2017). The Neurovascular Unit Coming of Age: A Journey through Neurovascular  
6 Coupling in Health and Disease. *Neuron*, 96(1), 17-42.  
7 <https://doi.org/10.1016/j.neuron.2017.07.030>

8 Iadecola, C., Duering, M., Hachinski, V., Joutel, A., Pendlebury, S. T., Schneider, J. A., & Dichgans, M.  
9 (2019). Vascular Cognitive Impairment and Dementia: JACC Scientific Expert Panel. *J Am Coll  
10 Cardiol*, 73(25), 3326-3344. <https://doi.org/10.1016/j.jacc.2019.04.034>

11 Jefferies, W. A., Price, K. A., Biron, K. E., Fenninger, F., Pfeifer, C. G., & Dickstein, D. L. (2013).  
12 Adjusting the compass: new insights into the role of angiogenesis in Alzheimer's disease.  
13 *Alzheimers Res Ther*, 5(6), 64. <https://doi.org/10.1186/alzrt230>

14 Kapasi, A., DeCarli, C., & Schneider, J. A. (2017). Impact of multiple pathologies on the threshold for  
15 clinically overt dementia. *Acta Neuropathol*, 134(2), 171-186. [https://doi.org/10.1007/s00401-017-1717-7](https://doi.org/10.1007/s00401-<br/>16 017-1717-7)

17 Kapasi, A., & Schneider, J. A. (2016). Vascular contributions to cognitive impairment, clinical  
18 Alzheimer's disease, and dementia in older persons. *Biochim Biophys Acta*, 1862(5), 878-886.  
19 <https://doi.org/10.1016/j.bbadi.2015.12.023>

20 Kurth, T., Rist, P. M., Ridker, P. M., Kotler, G., Bubes, V., & Buring, J. E. (2020). Association of Migraine  
21 With Aura and Other Risk Factors With Incident Cardiovascular Disease in Women. *JAMA*,  
22 323(22), 2281-2289. <https://doi.org/10.1001/jama.2020.7172>

23 Li, B., Lu, X., Moeini, M., Sakadzic, S., Thorin, E., & Lesage, F. (2019). Atherosclerosis is associated  
24 with a decrease in cerebral microvascular blood flow and tissue oxygenation. *PLoS One*, 14(8),  
25 e0221547. <https://doi.org/10.1371/journal.pone.0221547>

26 Livak, K. J., & Schmittgen, T. D. (2001). Analysis of relative gene expression data using real-time  
27 quantitative PCR and the 2(-Delta Delta C(T)) Method. *Methods*, 25(4), 402-408.  
28 <https://doi.org/10.1006/meth.2001.1262>

29 Lusis, A. J. (2000). Atherosclerosis. *Nature*, 407(6801), 233-241. <https://doi.org/10.1038/35025203>

30 Madisen, L., Mao, T., Koch, H., Zhuo, J. M., Berenyi, A., Fujisawa, S., Hsu, Y. W., Garcia, A. J., 3rd,  
31 Gu, X., Zanella, S., Kidney, J., Gu, H., Mao, Y., Hooks, B. M., Boyden, E. S., Buzsaki, G.,  
32 Ramirez, J. M., Jones, A. R., Svoboda, K., Han, X., Turner, E. E., & Zeng, H. (2012). A toolbox  
33 of Cre-dependent optogenetic transgenic mice for light-induced activation and silencing. *Nat  
34 Neurosci*, 15(5), 793-802. <https://doi.org/10.1038/nn.3078>

35 Matthews, F. E., Brayne, C., Lowe, J., McKeith, I., Wharton, S. B., & Ince, P. (2009). Epidemiological  
36 pathology of dementia: attributable-risks at death in the Medical Research Council Cognitive  
37 Function and Ageing Study. *PLoS Med*, 6(11), e1000180.  
38 <https://doi.org/10.1371/journal.pmed.1000180>

39 Mayhew, J., Zheng, Y., Hou, Y., Vuksanovic, B., Berwick, J., Askew, S., & Coffey, P. (1999).  
40 Spectroscopic analysis of changes in remitted illumination: the response to increased neural  
41 activity in brain. *Neuroimage*, 10(3 Pt 1), 304-326. <https://doi.org/10.1006/nimg.1999.0460>

42 Morton, R. E., St John, P. D., & Tyas, S. L. (2019). Migraine and the risk of all-cause dementia,  
43 Alzheimer's disease, and vascular dementia: A prospective cohort study in community-dwelling  
44 older adults. *Int J Geriatr Psychiatry*, 34(11), 1667-1676. <https://doi.org/10.1002/gps.5180>

45 Mucke, L., Masliah, E., Yu, G. Q., Mallory, M., Rockenstein, E. M., Tatsuno, G., Hu, K., Kholodenko,  
46 D., Johnson-Wood, K., & McConlogue, L. (2000). High-level neuronal expression of abeta 1-  
47 42 in wild-type human amyloid protein precursor transgenic mice: synaptotoxicity without  
48 plaque formation. *J Neurosci*, 20(11), 4050-4058.

49 Munting, L. P., Derieppe, M., Suijgeest, E., Hirschler, L., van Osch, M. J., Denis de Senneville, B., &  
50 van der Weerd, L. (2021). Cerebral blood flow and cerebrovascular reactivity are preserved in  
51 a mouse model of cerebral microvascular amyloidosis. *eLife*, 10.  
52 <https://doi.org/10.7554/eLife.61279>

53 Napoli, C., Witztum, J. L., de Nigris, F., Palumbo, G., D'Armiento, F. P., & Palinski, W. (1999).  
54 Intracranial arteries of human fetuses are more resistant to hypercholesterolemia-induced fatty  
55 streak formation than extracranial arteries. *Circulation*, 99(15), 2003-2010.  
56 <https://doi.org/10.1161/01.cir.99.15.2003>

57 Neuropathology Group. Medical Research Council Cognitive, F., & Aging, S. (2001). Pathological  
58 correlates of late-onset dementia in a multicentre, community-based population in England and  
59 Wales. Neuropathology Group of the Medical Research Council Cognitive Function and Ageing

1 Study (MRC CFAS). *Lancet*, 357(9251), 169-175. [https://doi.org/10.1016/s0140-6736\(00\)03589-3](https://doi.org/10.1016/s0140-6736(00)03589-3)

2 Rahimi, J., & Kovacs, G. G. (2014). Prevalence of mixed pathologies in the aging brain. *Alzheimers Res Ther*, 6(9), 82. <https://doi.org/10.1186/s13195-014-0082-1>

3 Ripa, P., Ornello, R., Pistoia, F., Carolei, A., & Sacco, S. (2015). Spreading depolarization may link 4 migraine, stroke, and other cardiovascular disease. *Headache*, 55(1), 180-182. <https://doi.org/10.1111/head.12436>

5 Roche-Molina, M., Sanz-Rosa, D., Cruz, F. M., Garcia-Prieto, J., Lopez, S., Abia, R., Muriana, F. J., 6 Fuster, V., Ibanez, B., & Bernal, J. A. (2015). Induction of sustained hypercholesterolemia by 7 single adeno-associated virus-mediated gene transfer of mutant hPCSK9. *Arterioscler Thromb Vasc Biol*, 35(1), 50-59. <https://doi.org/10.1161/ATVBAHA.114.303617>

8 Shabir, O., Berwick, J., & Francis, S. E. (2018). Neurovascular dysfunction in vascular dementia, 9 Alzheimer's and atherosclerosis. *BMC Neurosci*, 19(1), 62. <https://doi.org/10.1186/s12868-018-0465-5>

10 Shabir, O., Sharp, P., Rebollar, M. A., Boorman, L., Howarth, C., Wharton, S. B., Francis, S. E., & 11 Berwick, J. (2020). Enhanced Cerebral Blood Volume under Normobaric Hyperoxia in the J20-hAPP 12 Mouse Model of Alzheimer's Disease. *Sci Rep*, 10(1), 7518. <https://doi.org/10.1038/s41598-020-64334-4>

13 Sharp, P. S., Ameen-Ali, K. E., Boorman, L., Harris, S., Wharton, S., Howarth, C., Shabir, O., Redgrave, 14 P., & Berwick, J. (2019). Neurovascular coupling preserved in a chronic mouse model of 15 Alzheimer's disease: Methodology is critical. *J Cereb Blood Flow Metab*, 271678X19890830. <https://doi.org/10.1177/0271678X19890830>

16 Sharp, P. S., Shaw, K., Boorman, L., Harris, S., Kennerley, A. J., Azzouz, M., & Berwick, J. (2015). 17 Comparison of stimulus-evoked cerebral hemodynamics in the awake mouse and under a 18 novel anesthetic regime. *Sci Rep*, 5, 12621. <https://doi.org/10.1038/srep12621>

19 Taniguchi, H., He, M., Wu, P., Kim, S., Paik, R., Sugino, K., Kvitsiani, D., Fu, Y., Lu, J., Lin, Y., Miyoshi, 20 G., Shima, Y., Fishell, G., Nelson, S. B., & Huang, Z. J. (2011). A resource of Cre driver lines 21 for genetic targeting of GABAergic neurons in cerebral cortex. *Neuron*, 71(6), 995-1013. <https://doi.org/10.1016/j.neuron.2011.07.026>

22 Yemisci, M., & Eikermann-Haerter, K. (2019). Aura and Stroke: relationship and what we have learnt 23 from preclinical models. *J Headache Pain*, 20(1), 63. <https://doi.org/10.1186/s10194-019-1016-x>

24 Zlokovic, B. V. (2011). Neurovascular pathways to neurodegeneration in Alzheimer's disease and other 25 disorders. *Nat Rev Neurosci*, 12(12), 723-738. <https://doi.org/10.1038/nrn3114>

26